Chemical Science

ROYAL SOCIETY OF CHEMISTRY

EDGE ARTICLE

View Article Online
View Journal

Cite this: DOI: 10.1039/d5sc07682j

All publication charges for this article have been paid for by the Royal Society of Chemistry

Received 4th October 2025
Accepted 7th January 2026

DOI: 10.1039/d5sc07682j

rsc.li/chemical-science

Axially chiral thiophene scaffolds: configurational stability and circularly polarized luminescence

Xingyang Li, Shuai Qiu, Wan Xu,* Jia Tang, Zhiying Ma and Hua Wang *

A new type of axially chiral compound, 3,3′-bidithieno[2,3-*b*:3′,2′-*d*]thiophene (**BDTT**), bearing aryl groups (**BDTT-Ar**s) was synthesized and enantiomerically resolved. The racemization of enantiomers showed that their inversion barriers (ΔG) are in the range of 17.32–29.73 kcal mol^{-1}. Among them, **BDTT-9An** exhibited exceptional circularly polarized luminescence (CPL) properties, achieving a luminescence dissymmetry factor $|g_{lum}|$ up to 10^{-2}. This work provides critical theoretical insights into non-benzenoid axial chirality in novel optoelectronic materials.

Introduction

Axially chiral molecules with circularly polarized luminescence (CPL) have attracted significant research interest in the fields of organic chemistry, materials chemistry, polymer chemistry, supramolecular chemistry and bioscience due to their wide use in 3D information displays, biological probes, anti-counterfeiting and so forth.[1–5] In recent decades, axially chiral CPL systems have mainly focused on hexacyclic aromatic rings as the chiral source, such as binaphthyl derivatives,[6–10] *peri*-xanthenoxanthene derivatives,[11] biphenyl derivatives,[12–15], $[N–I–N]^+$-type halogen bonded dimers,[16] and C–N axial chirality systems.[17] However, the structural diversity and functional extensibility remain limited owing to a heavy reliance on conventional scaffolds.[18–24] This limitation has hampered the discovery of novel axially chiral skeletons and the advancement of CPL materials, consequently creating an urgent demand for rational molecular engineering to develop axially chiral systems that combine high-performance CPL with excellent configurational stability.

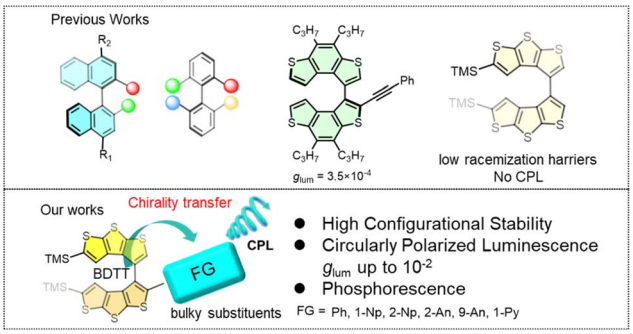

Fig. 1 The reported axial chirality molecules with CPL, and the designed **BDTT**-based axial chiral compounds (**BDTT-Ar**s): molecular structures with CPL properties.

Thiophene derivatives (Fig. 1) are versatile building blocks in materials chemistry and organic synthesis,[25,26] yet few axially chiral systems based on them have been realized. A rare example—3,3′-bi(benzo[*b*]thiophene-*S*,*S*-dioxide) derivatives—exhibits optical properties and configurational stability.[27] The scarcity of such scaffolds stems from the difficulty in constructing configurationally stable axially chiral structures from five-membered heteroaromatic rings. This challenge is further illustrated by recent axially chiral systems based on azoles,[28,29] thiophene,[30] and related analogues,[31] which show CPL activity but suffer from low dissymmetry factors and low racemization barriers, undermining their long-term stability.

Thieno[2,3-*b*:3′,2′-*d*]thiophene (**DTT**) is a key building block for thiophene-based [n]helicenes[32–34] and organic electronics such as OLEDs[35,36] and OFETs.[37] Its dimer, **BDTT**, was previously identified by us as a novel axially chiral scaffold,[38,39] but its low racemization barrier has precluded the development of its chiroptical properties, particularly circularly polarized luminescence (CPL). To address this issue, we leveraged the well-defined α-sites of **BDTT** to install aryl substituents of varying sizes (Fig. 1). This molecular design serves a dual purpose: sterically enhancing the configurational stability by modulating the atropisomerism energy barrier, and introducing high-fluorescence quantum yield fluorophores to transfer the axial chirality into CPL emission. Herein, we report the design and synthesis of this **BDTT** series, successfully granting them attractive CPL properties.

Results and discussion

Construction of BDTT-Ars

The synthetic route to the target **BDTT**-based axially chiral compounds (**BDTT-Ar**s) is delineated in Scheme 1. The axially

Institute of Nanoscience and Engineering, Henan University, Kaifeng, 475004, P. R. China. E-mail: 40070005@henu.edu.cn; hwang@henu.edu.cn

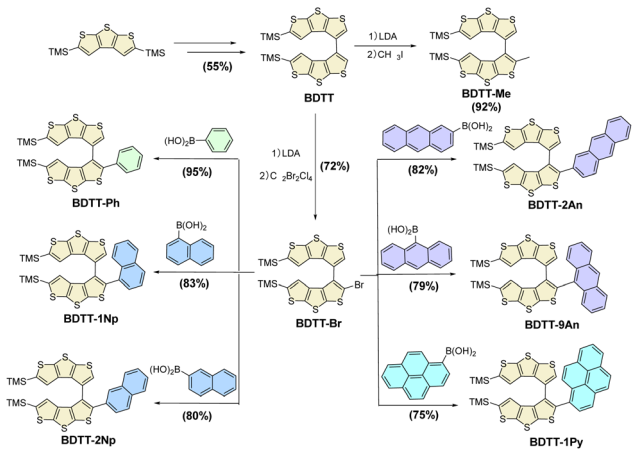

Scheme 1 Synthetic route to BDTT-Ars.

chiral precursor **BDTT** was synthesized *via* Li/Br exchange of (4-bromodithieno[2,3-*b*:3′,2′-*d*]thiophen-2-yl)trimethylsilane-(**BDTT**) and subsequent oxidation with $CuCl_2$. **BDTT** was deprotonated by LDA and then quenched with $C_2Br_2Cl_4$ to give (2-bromo-[3,3′-bidithieno[2,3-*b*:3′,2′-*d*]thiophene]-5,5′-diyl)bis(trimethylsilane) (**BDTT-Br**) in 85% yield. After intermolecular Suzuki coupling reactions for arylation between **BDTT-Br** and **Ar**-Bpin, the target products **BDTT-Ph**, **BDTT-1Np**, **BDTT-2Np**, **BDTT-2An**, **BDTT-9An** and **BDTT-1Py** were generated with yields of 95%, 83%, 80%, 82%, 73% and 75%, respectively. The relatively low yields of **BDTT-9An** and **BDTT-1Py** are attributed to the reduced coupling efficiency caused by their significant steric hindrance. The molecular structures of all target compounds, **BDTT-Ar**s are confirmed by ^{1}H NMR, ^{13}C NMR, HRMS and IR spectra (see the SI).

Spectroscopic features and electrochemical properties

The UV-Vis absorption spectra of **BDTT-Me** and all **BDTT-Ar**s exhibit two major absorption bands within 220–300 nm (band I) and 310–400 nm (band II). Gradual substitution of the α-H of **BDTT** with functional groups of different sizes in **BDTT-Ar**s from methyl to pyrene leads to a modest shift in the main absorption peaks located at 313, 314, 319, 328, 329, 380 and 352 nm, respectively (Fig. 2a, and S40). This phenomenon is attributed to the enhanced conjugation of the axially chiral molecule with increasing size of the functional substituent, and the absorption peaks in band II are assigned to HOMO → LUMO transitions. Cyclic voltammetry (CV) behaviors of **BDTT-Ar**s showed only one reversible oxidation wave at E_1° = +1.38 V for **BDTT-Ph**, E_1° = +1.32 V for **BDTT-9An** and E_1° = +1.58 V for **BDTT-1Py**, while **BDTT-1Np**, **BDTT-2Np** and **BDTT-2An** showed two reversible oxidation waves at E_1° = +1.37 V and E_2° = +1.62 V for **BDTT-1Np**, E_1° = +1.34 V and E_2° = +1.67 V for **BDTT-2Np** and E_1° = +1.24 V and E_2° = +1.58 V for **BDTT-2An** (*vs.* Fc/Fc$^+$, Fig. S15). Based on the first oxidation potentials, the HOMO energy levels were calculated to be −5.70 eV for **BDTT-Ph**, −5.68 eV for **BDTT-1Np**, −5.62 eV for **BDTT-2Np**, −5.53 eV for **BDTT-2An**, −5.50 eV for **BDTT-9An**, and −5.45 eV for **BDTT-1Py** (Table S15). With gradually increasing HOMO levels, the optical band gaps gradually narrow. Quantum chemistry calculations were employed to further predict the energy levels and electron-cloud distributions of the HOMO and LUMO orbitals for **BDTT-Ar**s. As presented in Fig. S45, **BDTT-Ar**s possess similar HOMO and LUMO distributions, with the HOMOs mainly distributed over the aromatic functional group and a small portion on the **DTT**s, while the LUMOs are distributed over the aromatic functional group. The calculated HOMO and LUMO levels are consistent with the experimental values.

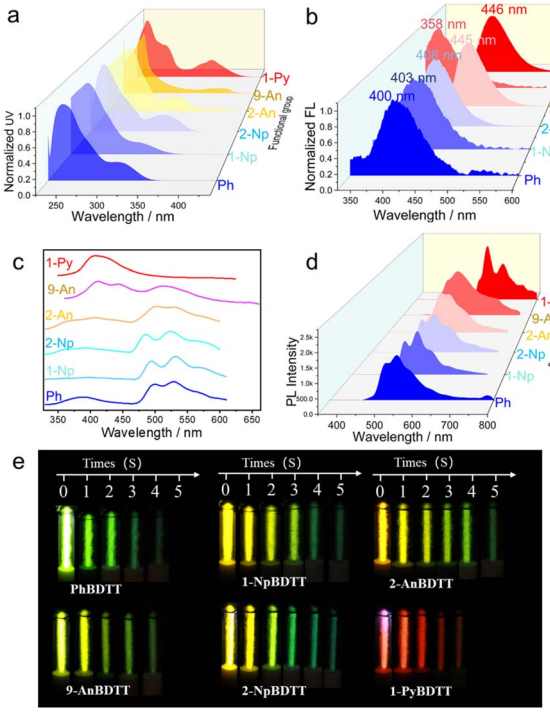

Fig. 2 a) Absorption spectra and (b) PL spectra of **BDTT-Ar**s in DCM, [C] = 1.0 × 10^{-5} M. (c) Steady state photoluminescence spectra and (d) delayed emission spectra of **BDTT-Ar**s in 2-MTHF ([C] = 1.0 × 10^{-5} M) at 77 K (0.5 ms, delayed). (e) Long afterglow photographs of **BDTT-Ar**s in 2-MTHF in quartz tubes at 77 K under irradiation of a 365 nm lamp (5 W).

The FL spectra of **BDTT-Ar**s are shown in Fig. 2b. As anticipated, **BDTT**, **BDTT-Br**, and **BDTT-Me** exhibit fluorescence emission that is too weak to be detected due to the heavy-atom effect of sulfur atoms. However, **BDTT-Ar**s emit intense blue emission in degassed dilute dichloromethane (DCM) solution. Their emission peaks are located at 400 (Φ = 0.03%), 403 (Φ = 0.06%), 408 (Φ = 0.32%), 445 (Φ = 0.47%), 358 (Φ = 0.19%) and 446 nm (Φ = 0.59%) for **BDTT-Ph**, **BDTT-1Np**, **BDTT-2Np**, **BDTT-2An**, **BDTT-9An** and **BDTT-1Py** in DCM solution respectively, in line with the trend in λ_{abs} (Fig. 2a). In the solid state, with the gradual increase of the Ar size, the fluorescence quantum yields of **BDTT-Ar**s increased due to the increase of intermolecular interactions among Ar moieties.

It is noteworthy that **BDTT-9An** exhibits the bluest emission, which can be attributed to the poor conjugation induced by the 9-substituted anthracene and the **DTT** moiety with a large dihedral angle between them. Moreover, the fluorescence quantum yield increases with the extension of substituent

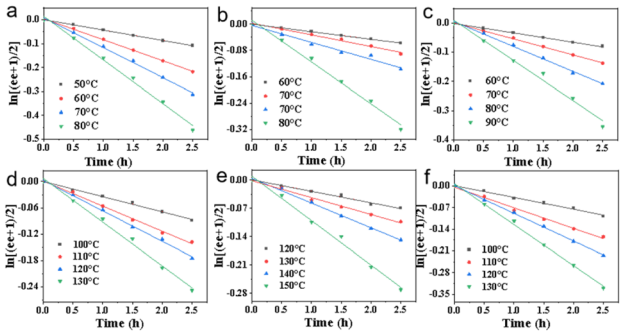

Fig. 3 Kinetic measurements of the racemization of BDTT-Ars (a–f: BDTT-Ph, BDTT-1Np, BDTT-2Np, BDTT-2An, BDTT-9An and BDTT-1Py, respectively).

Table 1 The activation kinetic parameters ΔH and ΔS of BDTT-Ars and BDTT-Me

Compound	ΔH/kcal mol^{-1}	ΔS/J k^{-1}	ΔG/kcal mol^{-1}
BDTT-Me	14.68	14.67	13.72
BDTT-Ph	17.47	2.31	17.32
BDTT-1Np	23.24	6.77	22.8
BDTT-2Np	21.26	6.9	20.9
BDTT-2An	24.96	1.92	24.83
BDTT-9An	30.26	8.18	29.73
BDTT-1Py	28.13	8.36	27.58

conjugation, demonstrating that **BDTT-Ar**s can serve as excellent candidates for CPL materials. As previously reported in our work,[32] the heavy atomic effect of sulfur atoms can promote the decay of intersystem crossing (ISC), resulting in more efficient phosphorescence intensity. However, no phosphorescence emission phenomena were observed in the solid powder of **BDTT-Ar**s due to their high non-radiative rate (Table S15). Fortunately, we observed dual emission peaks of **BDTT-Ar**s in 2-methyltetrahydrofuran (2-MTHF) at 77 K. The emission peaks in the short-wavelength region correspond to their local fluorescence emission, while the long-wavelength emission peaks (541, 543, 538, 546, 528, and 656 nm for **BDTT-Ph**, **BDTT-1Np**, **BDTT-2Np**, **BDTT-2An**, **BDTT-9An** and **BDTT-1Py**, respectively) were tentatively assigned to their phosphorescence emission (Fig. 2c). To verify this hypothesis, a 0.5 ms gated detection was applied in the detection of the samples. It was observed that the short-wavelength peaks disappeared, while the long-wavelength peaks remained (Fig. 2d), confirming their long-lived nature. Further lifetime measurements of the long-wavelength emission peak revealed lifetimes in the millisecond range (Fig. S47 in SI). Additionally, all samples exhibited an afterglow phenomenon lasting several seconds at 77 K (Fig. 2e). Theoretical calculations further confirm the existence of an efficient intersystem crossing (ISC) pathway between the singlet and triplet states in the **BDTT-Ar** molecules (Fig. S48). These experimental results demonstrate that the sulfur atoms in **BDTT-Ar**s can facilitate the ISC process, showing significant potential as phosphorescent materials.

Resolution of BDTT-Ars and barrier for racemization

Racemates **BDTT-Ar**s were successfully resolved into the corresponding enantiomers by using HPLC on a chiral stationary phase column (Fig. S22–S43). The absolute configurations of these enantiomers were determined through comparison of the experimental CD spectra (Fig. 4). We performed the racemization process of enantiomers **BDTT-Ar**s in 1,2-dichlorobenzene by heating the enantiomers in a Schlenk tube at different temperatures. The process was monitored by chiral HPLC (CHIRALPAK®IB) to obtain the changes in *ee* values. The half-life times were measured from the plot of ln[(*ee* + 1)/2] *vs.* time, respectively. As shown in Fig. 3 and Table 1, clear linear relationships were observed in all of these plots, indicating that the racemization proceeds *via* a first order reaction.[40] Based on these plots, the activation free energy (ΔG), heat content (ΔH) and entropy (ΔS) of racemization were calculated as shown in Table 2. Based on the above results, it can be observed that as the size of the functional groups gradually increases, the racemization barrier of **BDTT-Ar**s progressively rises. Compared to other five-membered biaryl axially chiral compounds (ΔG = 23.18 kcal mol^{-1}), namely 3,3′-bibenzo[1,2-*b*:4,3-*b*′]dithiophenes,[27] **BDTT-Ar**s exhibit superior conformational stability, comparable to that of **BINOL** (ΔG = 23.9 kcal mol^{-1}). The above experimental results demonstrate that **BDTT-Ar**s possess good chiral stability and can serve as a non-benzenoid axially chiral scaffold for constructing chiral materials.

CD and CPL properties

The CD and CPL spectra of the enantiomers **BDTT-Ar**s are depicted in Fig. 4. Enantiomerically pure **BDTT-Ar**s exhibit obvious Cotton effects in the range of 220 to 400 nm, with the maximum positive Cotton effects peaking at 250 nm for **BDTT-**

Table 2 Optical and electrochemical data of BDTT-Ars

Compound	λ_{FL} (nm)	λ_{PL} (nm)	Φ_F (%)	τ_F (ns)	τ_P (ms)	$[\alpha]_D^{25}$	$\lvert g_{abs}\rvert$	$\lvert g_{lum}\rvert$
BDTT-Me	—	—	—	—	—	−173.1° + 155.2°	1.3×10^{-4}	—
BDTT-Ph	401	504, 534	0.03	0.87	10	−675.0° + 692.8°	1.4×10^{-4}	1.2×10^{-3}
BDTT-1Np	421	506, 542	0.06	2.1	8	−897.3° + 842.5°	3.0×10^{-4}	7.9×10^{-3}
BDTT-2Np	416	512, 548	0.32	2.7	4	−770.4° + 742.6°	2.6×10^{-4}	1.9×10^{-3}
BDTT-2An	432	528, 552	0.47	6.3	110	−1035.8° + 1002.2°	4.4×10^{-4}	2.7×10^{-3}
BDTT-9An	447	544	0.19	1.7	26	−1185.6° + 1180.2°	2.3×10^{-3}	1.1×10^{-2}
BDTT-1Py	446	614, 672	0.59	7.2	75	−1205.3° + 1242.1°	9.7×10^{-4}	6.0×10^{-3}

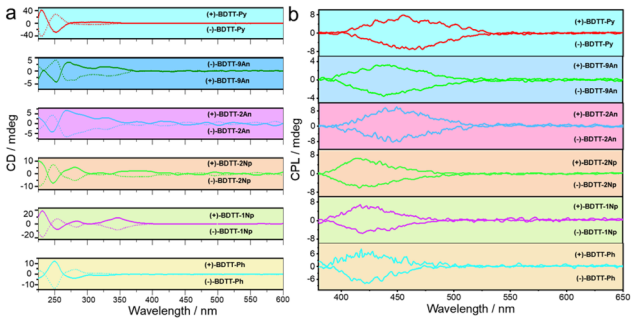

Fig. 4 Chiroptical properties. (a) CD and (b) CPL spectra of enantiomers **BDTT-Ar**s in DCM ([C] = 1×10^{-5} M).

Ph, 227 nm for **BDTT-1Np**, 273 nm for **BDTT-2Np**, 249 nm for **BDTT-2An**, 252 nm for **BDTT-9An**, and 231 nm for **BDTT-1Py**, respectively, with perfect mirror–image profiles in the CD spectra (Fig. 4a and Table 2). The CPL spectra of (+)-**BDTT-Ar**s and (−)-**BDTT-Ar**s showed perfect mirror image signals (Fig. 4b). As shown in Table 2, the luminescence dissymmetry factors (g_{lum}) of enantiomers **BDTT-Ar**s are listed. From the data in Table 2, we found that different substitution positions of the same substituent can lead to varying asymmetric factors in the enantiomers, for instance, $g_{\text{BDTT-1Np}} > g_{\text{BDTT-2Np}}$ and $g_{\text{BDTT-9An}} > g_{\text{BDTT-2An}}$. According to literature reports,[41] the dihedral angle of axially chiral molecules critically influences the asymmetric factor. Therefore, we attribute the observed differences to changes in the dihedral angles of **BDTT-Ar**s and the dipole moments of electric and magnetic transitions, caused by the steric effects of substituents at different positions. Among them, **BDTT-9An**, owing to its strongest steric hindrance, exhibits the highest asymmetric factor with g_{lum} up to 1.1×10^{-2} in **BDTT-Ar**s. These results demonstrate that efficient chirality transfer occurred in the molecules of **BDTT-Ar**s from the axially chiral **BDTT** moieties to the aryl moieties with high-fluorescence quantum yields and high performance CPL.[42,43]

Conclusions

In summary, the 3,3′-bidithieno[2,3-*b*:3′,2′-*d*]thiophene (**BDTT**) based axially chiral compounds (**BDTT-Ar**s) were successfully synthesized through oxidative coupling reaction and arylation. Incorporating size-varied aryl moieties into the axially chiral **BDTT** skeleton modulates their conformational stability, resulting in an increase in the racemization barrier with the increasing size of aryl substituents. Among them, **BDTT-9An** exhibits the highest racemization barrier of up to 29.73 kcal mol^{-1}, which is higher than that of **BINOL** (23.9 kcal mol^{-1}). Critically, the axially chiral **BDTT** scaffold enables efficient chirality transfer to functional substituents, conferring circularly polarized luminescence. And **BDTT-9An** exhibits the highest luminescence dissymmetry factor, reaching the order of 10^{-2} in solution. The chirality of **BDTT-Ar**s may be amplified in chiral supramolecular assemblies[44] or co-assemblies *via* fluorescence resonance energy transfer (FRET) processes.[45] Simultaneously, **BDTT-Ar**s demonstrate attractive phosphorescence emission at 77 K due to the heavy-atom effect of sulfur atoms in thiophene units. Collectively, this work represents the first systematic investigation of the chiroptical behaviors of **BDTT-Ar**s as a new axially chiral scaffold, providing critical theoretical insights into axial chirality in novel optoelectronic materials. And it also opens up intriguing possibilities for exploring the chiral stability and circularly polarized luminescence properties of **BDTT** upon functionalization at the two α-positions. Relevant studies are currently underway.

Author contributions

H. W. conceived the idea for this project. X. Y. L. performed the experiments. Z. Y. M., S. Q. and T. J. analyzed the data and theoretical calculations, and produced the artwork under the guidance of W. X. and H. W. All authors contributed to the manuscript preparation.

Conflicts of interest

There are no conflicts to declare.

Data availability

The data supporting this article have been included as part of the supplementary information (SI). Supplementary information is available. See DOI: https://doi.org/10.1039/d5sc07682j.

Acknowledgements

We thank Professor Hegui Gong for helpful discussion. This work was financially supported by the National Natural Science Foundation of China (22471061 and U2004213) and the Natural Science Foundation of Henan (242300421607 and 252300420754).

References

1 F. Song, Z. Zhao, Z. Liu, J. W. Y. Lam and B. Z. Tang, *J. Mater. Chem. C*, 2020, **8**, 3284–3301.
2 S.-P. Wan, H.-Y. Lu, M. Li and C. F. Chen, *J Photoch photobio C.*, 2022, **50**, 100500.
3 Y. Sang, J. Han, T. Zhao, P. Duan and M. Liu, *Adv. Mater.*, 2019, **32**, e1900110.
4 Z. L. Gong, X. Zhu, Z. Zhou, S. W. Zhang, D. Yang, B. Zhao, Y. P. Zhang, J. Deng, Y. Cheng, Y. X. Zheng, S. Q. Zang, H. Kuang, P. Duan, M. Yuan, C. F. Chen, Y. S. Zhao, Y. W. Zhong, B. Z. Tang and M. Liu, *Sci China Chem.*, 2021, **64**, 2060–2104.
5 P. Zhao, H. Y. Lu and C. F. Chen, *Chem. Soc. Rev.*, 2025, **54**, 8534–8554.
6 S. J. Brown, J. Zhao, E. Forehand, L. Dobrzycki, R. Roy, A. M. M. Hasan, W. Ding, C. Schaack and A. M. Evans, *J. Am. Chem. Soc.*, 2025, **147**, 3769–3775.
7 X. Mo, G. Chen, Y. Li, B. Xiao, X. Chen, X. Yin and C. Yang, *Chem. Sci.*, 2024, **15**, 17663–17670.
8 K. Takaishi, S. Murakami, K. Iwachid and T. Ema, *Chem. Sci.*, 2021, **12**, 14570.

9 L. Li, P. Jiang, X. Zhang and Y. Li, *Angew. Chem., Int. Ed.*, 2025, **64**, e202417149.
10 K. Wang, X. Ou, X. Niu, Z. Wang, F. Song, X. Dong, W. Guo, H.-Q. Peng, Z. Zhao, J. W. Y. Lam, J. Sun, H. Wu, S.-Y. Yu, F. Li and B. Z. Tang, *Aggregate*, 2025, **6**, e667.
11 K. Takaishi, S. Hinoide, T. Matsumoto and T. Ema, *J. Am. Chem. Soc.*, 2019, **141**, 11852–11857.
12 X. Z. Wang, S. Xing, X. Xiao, Li Yuan, Z. Y. Hou and Y. X. Zheng, *Adv. Funct. Mater.*, 2025, **35**, 2412044.
13 M. Wang and G. Zhou, *J. Org. Chem.*, 2025, **90**, 11510–11518.
14 Q. Wang, A. Pietropaolo, M. Fortino, Z. Song, M. Bando, N. Naga and T. Nakano, *Chirality*, 2021, **34**, 317–324.
15 X. Zhang, H. Ma, Q. Yin, F. Bai and Y. H. Chaolumen, *Org. Lett.*, 2025, **27**, 8969–8973.
16 S. An, A. Y. Hao and P. Y. Xing, *Chem. Sci.*, 2023, **14**, 10194–10202.
17 L. Zeng, C. H. Guo, C. Li, Z. W. Deng, Y. Lu, L. Lu, P. Meng, S. J. Sun, Z. J. Qiu, M. Li, Y. Xiong, Z. Zhao, C. F. Chen and B. Z. Tang, *Aggregate*, 2025, **6**, e70069.
18 Y. Yu, Y. Tang, S. Xu, Y. Lv, X. Hu and W. Tang, *Org. Lett.*, 2025, **27**, 6251–6256.
19 X. P. Wei, F. Gao, D. Li, Y. He, G. Li and X. J. Zhao, *Org. Lett.*, 2025, **27**, 1304–1309.
20 W. Ma, Z. Cao, N. Zhang, A. Hao and P. Xing, *Chem. Sci.*, 2025, **16**, 8405–8415.
21 W. L. Zhao, K. K. Tan, W. C. Guo, C. H. Guo, M. Li and C. F. Chen, *Adv. Sci.*, 2024, **11**, 2309031.
22 S. P. Wan, H. Y. Lu, M. Li and C. F. Chen, *J. Photochem. Photobiol.*, 2022, **50**, 100500.
23 Y. F. Wang, X. Liu, Y. Zhu, M. Li and C. F. Chen, *J. Mater. Chem. C*, 2022, **10**, 4805–4812.
24 X. Z. Wang, S. Xing, X. Xiao, L. Yuan, Z. Y. Hou and Y. X. Zheng, *Adv. Funct. Mater.*, 2024, **35**, 2412044.
25 S. Qiu, W. Li, S. Zhang, W. Xu, J. Tang, W. Tian and H. Wang, *Chem.–Eur. J.*, 2025, **31**, e202500554.
26 Z. Sun, W. Xu, S. Qiu, Z. Ma, C. Li, S. Zhang and H. Wang, *Chem. Sci.*, 2024, **15**, 1077–1087.
27 V. Pelliccioli, R. Franzini, G. Mazzeo, C. Villani, S. Abbate, G. Longhi, E. Licandro and S. Cauteruccio, *New J. Chem.*, 2021, **45**, 16442–16451.
28 K. Zhang, B. Zhang, L. Feng, L. He, C. F. Chen and M. Li, *Angew. Chem., Int. Ed.*, 2025, **64**, e202425094.
29 Y. Wang, K. Chen, H. Zhou, X. Chen and J. Xu, *Org. Lett.*, 2025, **27**, 7064–7069.
30 X. Bao, J. Rodriguez and D. Bonne, *Chem. Sci.*, 2020, **11**, 403–408.
31 S. Shaaban, H. Li, F. Otte, C. Strohmann, A. P. Antonchick and H. Waldmann, *Org. Lett.*, 2020, **22**, 9199–9202.
32 T. Qi, S. Guo, D. Wang, L. Li, Y. Liu and Y. Liu, *Dyes Pigments*, 2024, **235**, 112615.
33 S. Topal, O. S. Ipek, E. Sezer and T. Ozturk, *Chem.–Eng. J.*, 2022, **434**, 133868.
34 Z. X. Zhang, Z. F. Yu, M. J. Li and S. J. Zhen, *J. Mater. Chem. C*, 2025, **13**, 4480–4487.
35 B. H. Jiang, S. N. Afraj, Y. Ezhumalai, C. Y. Chang, Y. H. Yang, Y. W. Su, A. L. Abdelhady, Y. Q. Li, Z. E. Shi, C. L. Liu, M. C. Chen, H. M. Kao and C. P. Chen, *J. Mater. Chem. C*, 2024, **12**, 17966–17976.
36 K. Yang, Y. Mao, Z. Zhang, J. Xu, H. Wang, Y. He, P. Yu and Q. Song, *Nat. Commun.*, 2023, **14**, 4438.
37 S. X. Zhang, Z. Wu, D. Liu, Y. Zhao, S. J. Chen, Y. Wang and Y. Q. Liu, *Sci. China Mater.*, 2025, **68**, 1777–1787.
38 C. Li, J. Shi, L. Xu, Y. Wang, Y. Cheng and H. Wang, *J. Org. Chem.*, 2009, **74**, 408–411.
39 L. Dang, W. Xu, S. Qiu, Y. Yu, Z. Ma, L. Yue, H. Su, C. Li and H. Wang, *Org. Lett.*, 2024, **266**, 10141–10145.
40 M. Xu, S. Corio, J. Warnica, E. Kuker, A. Lu, J. Hirschi and V. Dong, *J. Am. Chem. Soc.*, 2025, **147**, 16270–16281.
41 K. Takaishi, S. Murakami, F. Yoshinami and T. Ema, *Angew. Chem., Int. Ed.*, 2022, **61**, e202204609.
42 D. Amsallem, A. Kumar, R. Naaman and O. Gidron, *Chirality*, 2023, **35**, 562–568.
43 W. Liu, J. Chen and W. Dou, *J. Phys. Chem. C*, 2025, **129**, 10181–10188.
44 H. Shang, Z. Ding, Y. Shen, B. Yang, M. Liu and S. Jiang, *Chem. Sci.*, 2020, **11**, 2169–2174.
45 T. Zhao, J. Han, P. Duan and M. Liu, *Acc. Chem. Res.*, 2020, **53**, 1279–1292.